Carbohydrate Polymers 280 (2022) 119025

Contents lists available at ScienceDirect

Carbohydrate Polymers

journal homepage: www.elsevier.com/locate/carbpol

Synergistic effects of antimicrobial peptide dendrimer-chitosan polymer conjugates against *Pseudomonas aeruginosa*

Viorica Patrulea [a,b,c,*], Bee-Ha Gan [d], Karl Perron [a,e], Xingguang Cai [d], Philippe Abdel-Sayed [f], Emmanuelle Sublet [a,b], Verena Ducret [e], Natalia Porroche Nerhot [a,b], Lee Ann Applegate [f], Gerrit Borchard [a,b], Jean-Louis Reymond [d,**], Olivier Jordan [a,b,***]

[a] University of Geneva, Institute of Pharmaceutical Sciences of Western Switzerland, 1, Rue Michel Servet, 1205 Geneva, Switzerland
[b] University of Geneva, Section of Pharmaceutical Sciences, 1, Rue Michel Servet, 1205 Geneva, Switzerland
[c] University of Oxford, Institute of Biomedical Engineering Science, Oxford OX3 7DQ, UK
[d] Department of Chemistry and Biochemistry, University of Bern, Freiestrasse 3, 3012 Bern, Switzerland
[e] Microbiology Unit, Department of Botany and Plant Biology, University of Geneva, 1211 Geneva, Switzerland
[f] Lausanne University Hospital (CHUV), Regenerative Therapy Unit, Service of Plastic, Reconstructive and Hand Surgery, EPCR Chemin des Croisettes 22, 1066 Epalinges, Switzerland

ARTICLE INFO

Keywords:
Multidrug-resistant bacteria
Antimicrobial peptide dendrimers (AMPDs)
Synergistic antimicrobial activities
Antimicrobial formulations
Wound infections

ABSTRACT

We report herein a new chemical platform for coupling chitosan derivatives to antimicrobial peptide dendrimers (AMPDs) with different degrees of ramification and molecular weights *via* thiol-maleimide reactions. Previous studies showed that simple incorporation of AMPDs to polymeric hydrogels resulted in a loss of antibacterial activity and augmented cytotoxicity to mammalian cells. We have shown that coupling AMPDs to chitosan derivatives enabled the two compounds to act synergistically. We showed that the antimicrobial activity was preserved when incorporating AMPD conjugates into various biopolymer formulations, including nanoparticles, gels, and foams. Investigating their mechanism of action using electron and time-lapse microscopy, we showed that the AMPD-chitosan conjugates were internalized after damaging outer and inner Gram-negative bacterial membranes. We also showed the absence of AMPD conjugates toxicity to mammalian cells. This chemical technological platform could be used for the development of new membrane disruptive therapeutics to eradicate pathogens present in acute and chronic wounds.

1. Introduction

Multidrug-resistant (MDR) bacteria remain an unresolved global public health issue, with the last-resort treatment based on polymyxins (Siriwardena, Stach, et al., 2018b), (Caires et al., 2019). Opportunistic *Pseudomonas aeruginosa* is one of the most challenging in the MDR bacterial collection, called ESKAPE (*Enterococcus faecium*, *Staphylococcus aureus*, *Klebsiella pneumoniae*, *Acinetobacter baumannii*, *Pseudomonas aeruginosa*, and *Enterobacter species*) (de la Cruz-Hernández et al., 2020), and is a common cause of hospital-acquired infections such as in severe burns (Abdel-Sayed et al., 2016) and immunocompromised patients (Chin et al., 2018). MDR *P. aeruginosa* exhibits a high incidence of antibiotic resistance, even to polymyxins (Krishnamurthy et al., 2019), which frequently cause nephrotoxicity and neurotoxicity (Caires et al., 2019). The overall number of antibiotics to fight against ESKAPE pathogens is declining due to high prevalence of antimicrobial resistance found against most of the current available drugs. *P. aeruginosa* and *A. baumannii* are mostly responsible for an increased nosocomial outbreak as they developed high resistance against many of the available antibiotics, mostly *via* chromosomal-mediated mutations (Kawano et al., 2020; Mulani et al., 2019; Wieland et al., 2018).

Skin is the primary body barrier against pathogens. However, wound infections, in particular *P. aeruginosa*-infected, are a major cause of mortality, morbidity and delayed wound healing (Abdel-Sayed et al.,

* Correspondence to: V. Patrulea, University of Geneva, Institute of Pharmaceutical Sciences of Western Switzerland, 1, Rue Michel Servet, 1205 Geneva, Switzerland.
** Corresponding author at: University of Bern, Department of Biochemistry, Freiestrasse 3, 3012 Bern, Switzerland.
*** Correspondence to: O. Jordan, University of Geneva, Section of Pharmaceutical Sciences, 1, Rue Michel Servet, 1205 Geneva, Switzerland.
E-mail address: olivier.jordan@unige.ch (O. Jordan).

https://doi.org/10.1016/j.carbpol.2021.119025
Received 16 September 2021; Received in revised form 19 November 2021; Accepted 14 December 2021
Available online 23 December 2021

2019). Although existing dressings may promote wound healing, they offer little protection against bacterial infections (Abdel-Sayed et al., 2016). On the other hand, current antimicrobial dressings may show some degree of cytotoxicity, which can hinder wound healing. Therefore, there is clearly an unmet clinical need to develop antimicrobial agents that could successfully eradicate *P. aeruginosa* without causing side effects.

To address this issue, antimicrobial peptides (AMPs) of natural and synthetic origin can be very efficient against a broad spectrum of bacteria (Gan et al., 2021; Xu et al., 2020), although they are rapidly degraded once in contact with human serum and therefore lose their activity (Costa et al., 2011; Rončević et al., 2019). Moreover, most of them are toxic and have a short half-life – the median half-life of the Food and Drug Administration (FDA)-approved peptides is as short as 9 h (Chen & Lu, 2020; Costa et al., 2011). The recently developed antimicrobial peptide dendrimers (AMPDs) have shown stronger spectrum and higher antibacterial activity than AMPs (Siriwardena, Stach, et al., 2018b). Compared to linear AMPs, AMPDs have a 3D, regularly branched structure formed by covalent bonds between amino acids and a higher density of surface groups (Kawano et al., 2020; Patrulea et al., 2020). The recently developed G3KL, a highly potent AMPD composed of L-lysine and *L*-leucine, shows high activity against MDR clinical isolates *P. aeruginosa* and *A. baumannii* (Siriwardena, Capecchi, et al., 2018a), such as poor stability in human serum of only a few hours.

Several strategies have been proposed to improve the efficacy and decrease the *in vivo* degradation and toxicity of antimicrobial agents (Costa et al., 2011; Kawano et al., 2020; Patrulea et al., 2020; Thapa et al., 2020). Approaches such as the optimization of peptide sequences may help to improve the efficacy/toxicity balance, peptide PEGylation may extend the half-life in serum, and peptide encapsulation into carriers may protect against proteolytic degradation. Nevertheless, these enhancements have led to little or no clinical translation. In this context, an emerging alternative strategy, the conjugation of AMPs to polymers, may hold promise to protect the peptide from degradation and/or to sustain its activity at the diseased site (Drayton et al., 2020; Mahlapuu et al., 2020; Nordström & Malmsten, 2017; Teixeira et al., 2020).

There is an important need to develop a long-lasting and efficient arsenal of AMPD-based formulations that may be used as topicals for chronic wounds (including venous, arterial and diabetic), nonhealing wounds, burns and even small surgery wounds that are prone to form biofilms. In this context, the purpose of this study is to develop a safe delivery system bearing AMPDs with strong antimicrobial effect. Knowing that AMPDs are already effective on their own but limited due to their poor proteolytic stability (Siriwardena, Capecchi, et al., 2018a; Siriwardena, Stach, et al., 2018b), we developed a chitosan-based platform intended to protect the active AMPD from its environment and thus extend its half-life and antimicrobial activity. Chitosan is a natural biopolymer, regarded as a safe material for wound healing (Patrulea et al., 2016; Patrulea, Ostafe, Borchard, and Jordan, 2015b), and thus can be used as a chemical platform to couple different molecules benefiting from its functional groups, such as amino and hydroxyl groups (Patrulea, Applegate, Ostafe, Jordan, and Borchard, 2015a). Herein, we functionalized chitosan derivatives (*O,O*-carboxymethyl-*N,N,N*-trimethyl chitosan (CMTMC) and *O,O*-carboxymethyl chitosan (CMC)) with large molecules such as AMPDs *via* thiol-maleimide reaction and further showed that the AMPD-chitosan conjugates eradicate *P. aeruginosa*. This chemistry allows tight control of the amount of grafted peptides to balance efficacy *versus* toxicity.

To the best of our knowledge, this study is the first report of the controlled chemical grafting of bulky AMPDs molecules to chitosan derivatives *via* covalent coupling chemistry. Bacterial membrane disruption with rapid killing kinetics by G3KL-chitosan conjugates was confirmed by TEM and SEM. Importantly, G3KL-chitosan conjugates were shown to be safe and nontoxic to mammalian cells *in vitro* and *ex vivo*.

Furthermore, synergistic effects that were observed upon coupling the two molecules encouraged us to design three different formulations including nanoparticles, gels and foams for the treatment of infected wounds. All the developed formulations exerted potent activity against *P. aeruginosa in vitro,* showing high biological activity of the AMPD-chitosan conjugates embedded into wound dressings.

2. Materials and methods

2.1. Chitosan derivatives synthesis: DAH-CMTMC and DAH-CMC

All the chemicals were purchased from Sigma Aldrich and used as received if not specified. The diaminohexane-*O,O*-carboxymethyl-*N,N,N*-trimethyl-chitosan (DAH-CMTMC) was prepared following previous protocols (Patrulea et al., 2016; Patrulea, Applegate, Ostafe, Jordan, and Borchard, 2015a), starting from chitosan (81% degree of deacetylation, ChitoClear Cg10, 8 mPa·s, Primex, Siglufjörður, Iceland) as depicted in Scheme 1.

The diaminohexane-*O,O*-carboxymethyl-chitosan (DAH-CMC) derivative was obtained similarly to DAH-CMTMC in two steps (carboxymethylation and spacer addition) with small modifications (Scheme 1). Carboxymethylation starts directly from pure chitosan without the dimethylation and trimethylation steps used for the DAH-CMTMC derivative. Subsequently, a 1,6-diamino-hexane (DAH) spacer was added to *O,O*-carboxymethylated chitosan (CMC) according to our previous report (Patrulea et al., 2016). Their structures were confirmed by ^{1}H NMR and FTIR as shown in Figs. 2 and 3.

2.2. Chemical platform for coupling AMPDs

As the direct addition of G3KL (G3 refers to generation 3) to biopolymer dressings hindered the antimicrobial activity of AMPD, we hypothesized that direct coupling of the peptide to chitosan-based biopolymers might preserve its activity, benefiting from chitosan safety, wound healing promotion and bacteriostatic properties. We therefore devised a strategy to covalently link our AMPDs to chitosan derivatives. To synthesize chitosan derivatives, such as CMTMC and CMC, we used previously developed protocols (Patrulea et al., 2016; Patrulea, Applegate, Ostafe, Jordan, and Borchard, 2015a). Furthermore, CMTMC derivatives can be used for the formation of nanoparticles upon coacervation process. In addition, adding a 6-carbon spacer DAH between CMTMC or CMC and AMPD gives more flexibility to the AMPD and thus could better display its properties. The addition of the DAH spacer led to two different chitosan derivatives, DAH-CMTMC and DAH-CMC, synthesized as illustrated in Scheme 1, following previously reported protocols (Patrulea et al., 2016; Patrulea, Applegate, Ostafe, Jordan, and Borchard, 2015a). To our knowledge, DAH coupling to CMC has not been reported before.

DAH-CMTMC has two additional steps compared to DAH-CMC, consisting of dimethylation and trimethylation steps. Subsequent reaction steps were similar for both DAH-CMTMC and DAH-CMC, namely, carboxymethylation and the addition of the 1,6-diaminohexane (DAH) spacer (Patrulea et al., 2016). Finally, AMPD was covalently attached to two chitosan derivatives using 7 different sulfo-crosslinkers that are heterobifunctional, water soluble and thiol-amine specific to enable coupling between amino-terminated chitosan-DAH and AMPD-cysteine (AMP-cys) *via* thiol-maleimide chemistry and "solvent-free" methods.

DAH-CMTMC is positively charged due to a quaternary amine that can serve as the counter ion for the preparation of nanoparticles by complexation with a negatively charged polymer (Patrulea et al., 2019). DAH-CMC is less positively charged and is a viable alternative for coupling to AMPDs when nanoparticles are not targeted. ^{1}H NMR and FTIR analysis confirmed the presence of each functional group for every step of the reaction (Figs. 2 and 3). Taken together, the coupling of AMPDs to chitosan derivatives is a very well-controlled reaction for the successful grafting of such highly branched peptides.

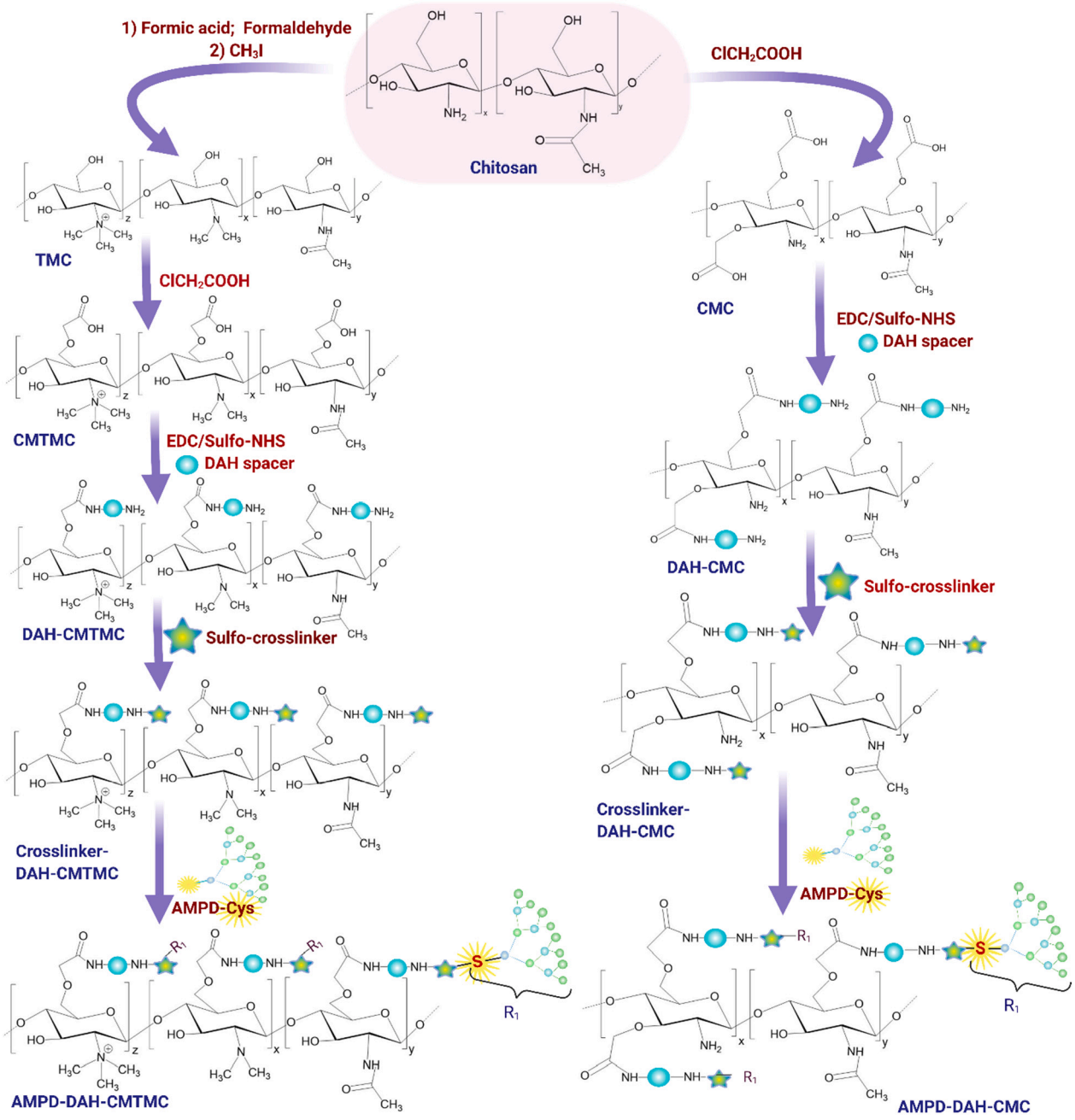

Scheme 1. Overview of the synthesis of chitosan derivatives (DAH-CMC and DAH-CMTMC) and their coupling to branched AMPD (G3KL) through 7 different sulfo-crosslinkers that are heterobifunctional, water soluble and thiol-amine specific to enable coupling between amino-terminated chitosan-DAH and AMPD-cysteine (cys).

2.3. Sulfo-crosslinkers

We selected seven promising sulfo-crosslinkers (see their full structures in Fig. S1) to achieve AMPD grafting to chitosan derivatives: 4-(*N*-maleimidomethyl)cyclohexane-1-carboxylic acid 3-sulfo-*N*-hydroxysuccinimide (sulfo-SMCC); sulfosuccinimidyl 4-(*N*-maleimidophenyl) butyrate (sulfo-SMPB); sulfo-*N*-succinimidyl 4-maleimidobutyrate (sulfo-GMBS); *N*-(ε-maleimidocaproyloxy) sulfosuccinimide (sulfo-EMCS); *N*-(κ-maleimidoundecanoyloxy) sulfosuccinimide (sulfo-KMUS); sulfosuccinimidyl 6-[3′-(2-pyridyldithio) propionamido]hexanoate (sulfo-LC-SPDP) and sulfosuccinimidyl (4-iodoacetyl)aminobenzoate (sulfo-SIAB). All crosslinkers were purchased from Sigma Aldrich, Switzerland except sulfo-SIAB, which was obtained from Brunschwig (Basel, Switzerland).

2.4. Solid phase synthesis of the AMPD

The third-generation AMPDs: G3KLcys and fluo-G3KLcys (Figs. S2 and S3); second-generation: G2KLcys and linear peptide: SB1cys (Fig. S4 and S5) used in this study were synthesized as described previously (Baeriswyl et al., 2019; Siriwardena, Stach, et al., 2018b; Stach et al., 2014). Peptide synthesis was carried out either manually or with CEM Liberty Microwave peptide synthesizer. The compounds were obtained as lyophilized powders of pure acetate salts. Additionally, cysteine was added to each AMPD/AMP to enable further peptide-chitosan coupling.

2.5. Coupling of G3KLcys/Fluo-G3KLcys AMPD to DAH-CMC or DAH-CMTMC polymers

The coupling of AMPDs to chitosan derivatives (DAH-CMC or DAH-CMTMC, as briefly depicted in Scheme 1) was achieved using seven different heterobifunctional sulfo-crosslinkers *via* thiol-maleimide chemistry. Lyophilized DAH-CMC or DAH-CMTMC polymer (10 mg) was dissolved in 3 mL of borate buffer, pH 8.0, containing 0.05 M EDTA. Sulfo-crosslinkers (1.7 mg/mL dissolved in borate buffer, pH 8.0) were added at a molar ratio of 1:2 to DAH-CMC or DAH-CMTMC. The reaction was stirred in the dark for 1 h at 40 °C. Dialysis in Amicon tubes (10 kDa cutoff) was performed to remove any nonreacted crosslinker followed by solubilization in borate buffer (pH 8.0). First, to avoid the formation of disulfide bridges, the G3KLcys peptide was treated with *tris*(2-carboxyethyl) phosphine (TCEP) (molar ratio 1.2 to 1) and then added to the reaction mixture and prepared by stirring in the dark for 7 days at 50 °C. The polymer solution was purified in Amicon tubes and then lyophilized. The degree of peptide grafting was measured by amino acid analysis (AAA), as shown in Table S1.

2.6. Coupling of G2KLcys and SB1cys to DAH-CMC and DAH-CMTMC polymers via the two chosen crosslinkers

G2KLcys and SB1cys coupling to DAH-CMC or DAH-CMTMC was performed with only two out of seven selected sulfo-crosslinkers: sulfo-SIAB and sulfo-GMBS. This choice was based on the grafting efficiency and solubility at physiological pH. The synthesis was performed as previously mentioned for coupling G3KLcys to chitosan derivatives. The results for AAA, the degree of substitution (DS) and synergy levels are listed in Table S2.

2.7. Nuclear magnetic resonance (1H NMR) and Fourier transform infrared (FTIR) spectroscopy

^{1}H NMR spectra for DAH-CMTMC and DAH-CMC, including the intermediate steps were recorded using Bruker Avance III HD 600 MHz spectrometer, combined with a SamplJet automated sample charger (Bruker BioSpin, Rheinstetten, Germany). Prediction of NMR spectra was performed with Mnova software V8.1 (MestreNova, Santiago de Compostela, Spain). All analyses were recorded at room temperature. ^{1}H chemical shifts were reported as parts per million (ppm). The polymers were dissolved in D_2O containing 1% DCl.

The characteristic peaks were recorded using a FTIR spectrometer (Bruker, Tensor 27) equipped with attenuated total reflectance (ATR, Pike). The background spectrum was collected every time by measuring the response of the spectrometer without sample before running the sample. All FTIR spectra were recorded against KBr beam splitter by cumulating 32 scans in the range of 650–4000 cm^{-1}.

2.8. Amino acid analysis (AAA)

Quantification of the degree of grafting was performed using AAA. AAA was done by vacuum-hydrolysis over 22 h in 6 M HCl and 0.1% phenol (Kambhampati et al., 2019). Briefly, the samples (10 μg) were transferred in a hydrolysis tube and then 5 μL of Titriplex III solution (2 mg/mL) was added. The samples were dried in a Speed-Vac. Then, 200 μL of 6 M HCl was pipetted to the hydrolysis vessel. The tube was then flushed with nitrogen, transferred to the hydrolysis vessel, and dried under vacuum. At the end, a vacuum of 20–40 mm Hg was applied. The vessel was then heated at 115 °C in a heat block for 22 h. After hydrolysis, the vessel was immediately vented, and the sample was dried in a Speed-Vac and then coupled to phenyl isothiocyanate. Afterwards, the samples were dried and quantified by HPLC (Kambhampati et al., 2019). Hydrolyzed amount was 10 μg and injected 40%.

2.9. Determination of minimum inhibitory concentration (MIC) and minimum bactericidal concentration (MBC)

The antibacterial activities of AMPD-chitosan derivatives were determined using the standard broth microdilution method as described (Wiegand et al., 2008). Polymers were prepared separately in MHB medium (Oxoid, UK) at a concentration of 2048 μg/mL, and 100 μL of stock solution was added to the first well of the microplate followed by serial dilutions. Then, 100 μL of bacterial suspension (direct colony suspension into physiological water (0.9% NaCl) to McFarland 0.5, diluted 100× in MHB) was added to each well of the 96-well microplate (final concentration 1–5 × 10^5 UFC/mL). One column was used for sterility control (MHB alone) and another one for bacterial inoculation with no antimicrobial agent (growth control). All samples were incubated for 24 h at 37 °C to allow bacterial growth. Iodonitrotetrazolium chloride (INT, Sigma-Aldrich) was added to each well as a growth indicator and incubated for several hours (Eloff, 1998). MIC was defined as the lowest concentration of the antimicrobial agent to inhibit the growth of the pathogen. Gentamycin was used as a reference. MBC was determined by enumerating the surviving bacteria in the wells of the MIC plate after 24 h of incubation at 37 °C. Serial dilutions were performed in a neutralizing solution (Peptoned buffer water (Biomérieux) containing Tween 80 (3%) and Lecithin (0.3%)) and spread on Luria broth (Applichem) plates. CFUs were enumerated after 24 h of growth at 37 °C. MBC corresponds to 99.99% killing.

The bacterial reference strains used in this study were *P. aeruginosa* (ATCC 27853 and PAO1) for MIC and MBC experiments and *P. aeruginosa* PAO1 for microscopy analysis (transmission electron microscopy: TEM, scanning electron microscopy: SEM), serum stability and time-killing assay.

2.10. Serum stability assay

Samples were prepared at a concentration of 128 × MIC in 0.1 M Tris-HCl pH 7.4 buffer with 12.5% human serum (Sigma Aldrich, St. Louis, USA) and shaking at 200 rpm at 37 °C. Samples were then submitted to MIC assay (same as described above) after 0, 6, 12, 24 and 48 h of incubation with *P. aeruginosa* PAO1.

After incubation with human serum, samples were diluted to 256 μg/mL (G3KL and In65) or 1006.7 μg/mL (G3KLcys-DAH-CMTMC) in 300 μL MHB medium, added to the first well of 96-well plate followed by serial dilution by ½. The concentration of the bacteria was quantified by measuring absorbance at 600 nm and diluted to $OD_{600} = 0.022$ to a final concentration of 5 × 10^5 CFU/mL. The sample solutions (150 μL) were mixed with 4 μL diluted bacterial suspension with a final inoculation of about of 5 × 10^5 CFU. The plates were incubated at 37 °C until satisfactory growth (~18 h). For each test, a sterility control (MHB alone) and growth control (MHB with bacterial inoculum) was used.

2.11. Antimicrobial activity. Time-lapse microscopy

Time-lapse microscopy was performed using Leica TCS SP8 microscope (Leica Microsystems GmbH, Mannheim, Germany) as described previously (Gan et al., 2019). The microscope is equipped with a white light laser (WLL, 470–670 nm). All experiments were performed with an HCX PL APO 100×/1.40 oil objective and HyD detectors.

The localization of the peptide and its permeability to *P. aeruginosa* cytosolic membrane was performed by time-lapse live imaging. Exponential phase of PAO1 was harvested and adjusted to OD 1.0. Bacteria were washed once with M63 medium supplemented with 1 mM $MgSO_4$ and 10% glycerol and resuspended in 1 mL of M63 medium. Coverslip (Sigma Aldrich) was fixed on the coverslip holder (Aluminium based, from Zentrale Werkstatt, University of Bern, Switzerland). 30 μL of the bacteria were mixed together with 30 μL of 2.4% low-melting agarose (Low Melting, Nucleic Acid Recovery, Fisher Bioreagent, Fisher scientific) on the fixed coverslip and simultaneously a second coverslip

(Corning®, square, No. 1, W × L 18 mm × 18 mm, Sigma Aldrich) was placed on top. Once the agarose solidified, the upper coverslip was removed and washed three times with M63 medium to remove as much as possible the swimming bacteria. 960 μL of the medium containing propidium iodide (final concentration at 1 μg/mL) was added to coverslip holder. After focusing the cells, the movie was started and 40 μL of 1 mg/mL Fluo-G3KLcys-DAH-CMTMC (final concentration of 40 μg/mL) was added to the coverslip. Fluo-G3KLcys-DAH-CMTMC was excited by using 488 nm laser and propidium iodide (Ex. 535 nm and Em. 617 nm) by 561 nm laser.

2.12. Antimicrobial activity. Time-kill kinetics assay

Time-Kill kinetics against *P. aeruginosa* PAO1 was performed on G3KLcys-DAH-CMTMC and G3KL in MHB medium (Sigma Aldrich, Buchs, Switzerland) at concentrations of 2 × MIC and 4 × MIC at 37 °C. Untreated bacteria at 10^6 CFU/mL was used as a growth control.

The bacteria were grown overnight with shaking (180 rpm) in 5 mL LB (Sigma Aldrich, Buchs, Switzerland) medium at 37 °C, then diluted to OD_{600} 0.002 ($2•10^6$ CFU/mL) in fresh MHB medium. Sample concentrations equal to 4 × MIC or 8 × MIC were prepared in fresh MHB. A 100 μL of the adjusted bacterial concentration and 100 μL of samples were mixed in a 96-well microplate and incubated at 37 °C with shaking (180 rpm). Bacterial growth was quantified at 0, 0.5, 1, 2, 3, 4 and 5 h. The quantification was done by plating 10-fold dilutions of sample in sterilized 0.9% NaCl on LB agar plates. LB agar plates were incubated at 37 °C overnight and the CFU was counted at each time-point. The assay was performed in triplicate, repeated at least twice and the graph of the log CFU/mL was plotted against time.

2.13. Biocompatibility assay

For each of the scaffold (with/without AMPD-conjugates), a squared piece of 1 × 1 cm was fixed to the bottom of a 6-well microplate with a metallic insert. Subsequently, human dermal fibroblasts (HDF, human dermal progenitor cells, 12-week male donor) were provided personally from one author (LAL), in the Regenerative Therapy Unit from the Centre Hospitalier Universitaire Vaudois (CHUV, Lausanne, Switzerland) under informed donor consent (Ethics Committee Protocol #62/07, Lausanne, Switzerland) were dispensed on top and around the foams at density of 3000 cells/cm^2 in duplicates. Cell viability was assessed in standard incubators at 37 °C using a Giemsa staining (Sigma Aldrich, Switzerland) at two time points: day 5 and day 7.

2.14. Hemolysis

The hemolysis assay was performed following the literature (Siriwardena, Stach, et al., 2018b) to determine the lytic concentration. Briefly, stock solution of the selected AMPDs coupled to chitosan derivatives at 20 × MIC (minimal inhibitory concentration) in PBS were prepared and diluted by two-fold serial dilution in a flat-bottom 96-well plate. Defibrinated sheep blood SR0051B (Oxoid™) from Thermo Scientific™ was washed three times with phosphate-buffered saline (PBS) and diluted to 5% solution. Following, 50 μL of each sample was added to 50 μL red blood cells (RBCs) solution in a 96-well round bottom microplate and left for stirring (Orbit LS shaker, S2030-LS-B) at room temperature for 30 min. Afterwards, centrifugation at 4000 rpm was performed. Aliquots of 50 μL from the supernatant were transferred to a fresh 96-well microplate and mixed with 250 μL of pure ethanol. The amount of the hemoglobin released was measured at 412 and 700 nm. PBS and water for injection (WFI) were considered as 0% and 100% lysis, respectively.

In parallel, RBCs were prepared using defibrinated sheep blood (Oxoid Ltd. Thermo-Fischer). 200 μL of sheep blood were added to 1 mL of PBS, very gently mixed and centrifuged at 1500 rpm for 1–2 min. The plasma was discarded carefully with a pipette. The washing was repeated 2 times (until the color of the supernatant was clear) and the erythrocyte pellets were re-suspended in 11 mL PBS and then freshly used for the assay.

2.15. WST-1 proliferation assay

HDF cells were cultured in DMEM (Dulbecco's modified Eagle medium, Sigma Aldrich) supplemented with 10% fetal bovine serum (FBS, Invitrogen, Carlsbad, CA, USA), 1% NaPyr and 1% L-Glutamine (Sigma) without any antibiotic addition.

HDF were seeded in a 96-well plate (Corning®, USA) at a density of 6×10^3 cells/cm^2. To each well, 100 μL of cell suspension was added and incubated for 48 h. DMEM was then replaced by 100 μL of AMPD-chitosan derivative suspension within a range of concentrations of 1 to 20 × MIC. Cell viability under polymer incubation was evaluated during 2 and 4 days. SDS (1%) was used as negative control. The polymer solution was changed every three days. 100 μL of WST-1 (Roche, Switzerland) (1:10 dilution in DMEM) were added in each well after removing the polymer suspension and incubated for 1.5 h. Absorbance was recorded with a BioTek Microplate reader (GmbH, Luzern, Switzerland) at two different wavelengths (450 and 690 nm). The viability was presented as percentage compared to the positive control group (cells in DMEM supplemented with 10% FBS). All experiments were carried out in triplicates.

2.16. Statistical tests

Two-way ANOVA was used to analyze all *in vitro* assays with GraphPad Prism 6 (GraphPad Software Inc., La Jolla, USA), followed by Sidak's multiple comparison test to assess significance at a level $p < 0.05$. The results are expressed as the mean ± standard deviation ($n = 3$).

3. Results and discussion

3.1. Direct addition of AMPD to polymer bandages inhibits the antimicrobial activity of the peptide dendrimer

Since coupling peptides to polymers or surfaces may reduce their activity (Costa et al., 2011), we first added G3KL in solution, as depicted in Scheme 2, to a biopolymer mixture containing hyaluronic acid (HA) and CMC. To evaluate the prospect of using it as a wound dressing product, we assessed its efficacy against *P. aeruginosa*. Surprisingly, the MIC against *P. aeruginosa* was decreased by 64-fold, with inhibition of the activity of G3KL upon mixing it with HA and CMC dressings (Table 1). This could be due to a complexation process between positively charged G3KL and negatively charged HA or CMC. Therefore, potent AMPDs need appropriately designed systems to safely deliver them to the target site without altering their activity, providing stability over the wound healing period and potentially improving overall effectiveness.

3.2. Coupling G3KLcys to CMC and CMTMC leads to synergistic antimicrobial activities

To couple G3KL to chitosan derivatives, we functionalized the peptide dendrimer by adding one cys at the core. The addition of cys enabled the coupling of thiol groups from the AMPD to amine functional groups from the derivatized chitosan *via* thiol-maleimide Michael addition chemistry (Belbekhouche et al., 2016).

MIC is expressed as the μg equivalent of AMPD in the conjugate composition calculated based on the degree of substitution obtained from AAA (Table S1). The stars represent different levels of synergy of the conjugate with respect to G3KLcys and chitosan derivatives (very strong synergy (*****); strong synergy (****) and synergy (***)) calculated using the fractional inhibitory index (FIC) based on the Chou-Talalay method (Chou, 2006) (calculations shown in Table S1).

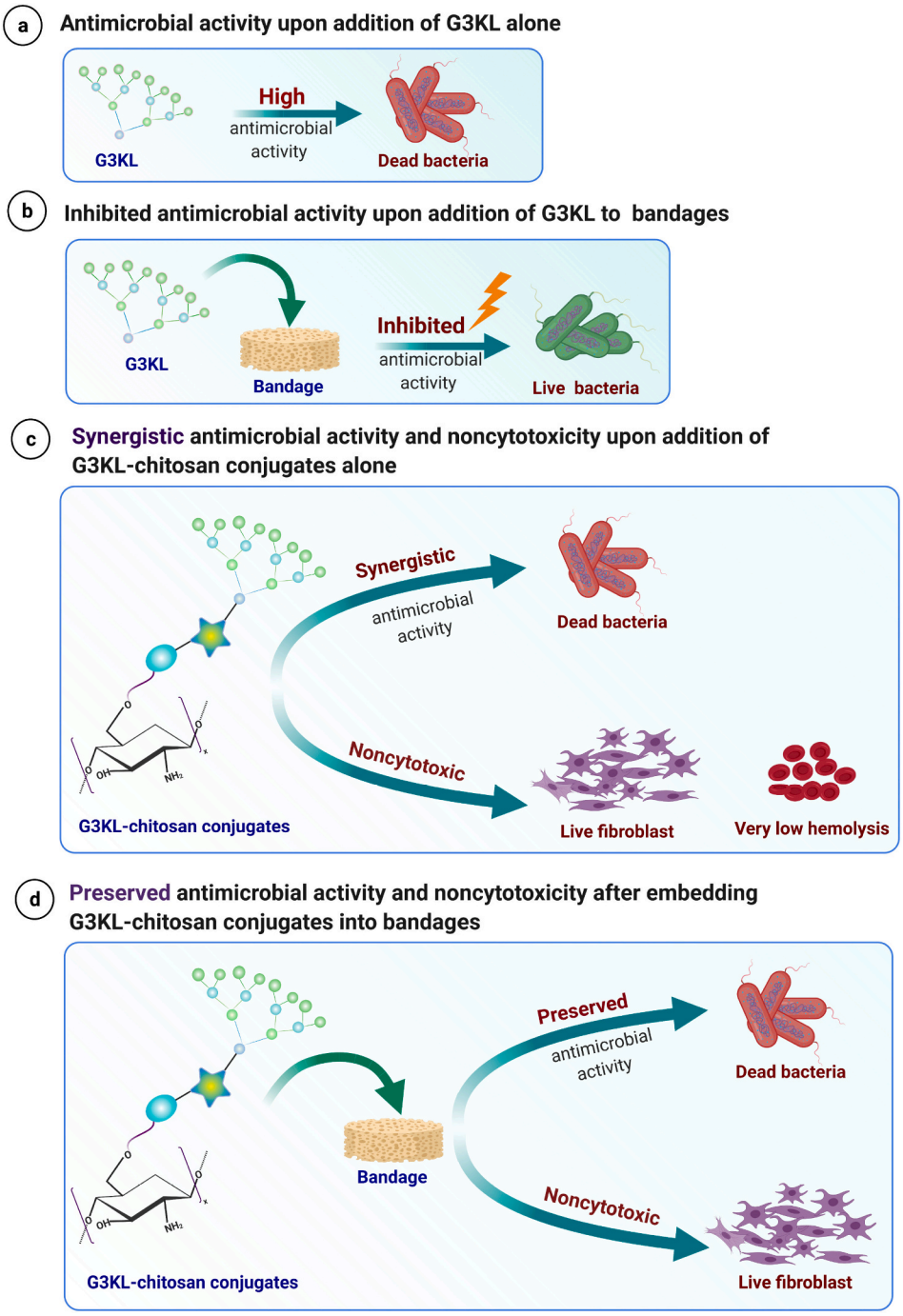

Scheme 2. Schematic illustration of the AMPD delivery approaches used in this study. a) G3KL AMPD killing effect on *P. aeruginosa*; b) Simple addition of G3KL AMPD to biopolymer dressings leads to a 32- to 64-fold inhibition of antimicrobial activity; c) Synergistic effect against *P. aeruginosa* obtained upon coupling AMPD to a chitosan derivative platform and d) Preserved antimicrobial activity upon incorporation of the AMPD conjugates into biopolymer dressings.

The influence of the crosslinker on antimicrobial activity was assessed by varying the length of the aliphatic chain of the crosslinker belonging to a structurally diverse range of reactive groups (*e.g.*, alkyl chain and/or addition of cyclohexane, phenyl, pyridyl-dithiol, amino-benzoate and iodoacetyl reactive groups). The sulfo-crosslinkers used herein are heterobifunctional, water-soluble amine-to-sulfhydryl cross-linking reagents with N-hydroxy-succinimide esters and maleimide or other reactive groups.

The results showed that conjugates with crosslinkers of shorter aliphatic chains, such as sulfo-GMBS, tended to improve the efficacy against *P. aeruginosa* (Fig. 1). Additional requirements for high solubility point out the interest of the sulfo-SIAB-CMTMC derivative. Increasing the alkyl chain of the crosslinker from propyl to decyl or adding other functional groups to the already existing 6-carbon spacer (González-Fernández et al., 2018) coupled to chitosan derivatives did not improve the antimicrobial activity. Importantly, the antibacterial activity of native G3KLcys (MIC: 16 μg/mL) is preserved during the reaction with chitosan derivatives *via* any of the chosen crosslinkers. Surprisingly, we found significantly higher antimicrobial activities for the conjugates for all crosslinkers used than for native AMPD. This suggests synergistic effects upon coupling the AMPD to chitosan. Using the Chou-Talalay method (Chou, 2006), the degree of synergy between G3KLcys and

Table 1
MIC (μg/mL) activities of G3KLcys AMPD or G3KLcys-chitosan conjugates against *P. aeruginosa* (PAO1 and ATCC 27853) upon addition to HA and CMC dressings.

Compound	MIC (μg/mL)	Conclusions
G3KLcys	8–16	
G3KLcys simple addition:		
HMW HA 1% + CMC 2% matrix	>TC[a]	G3KLcys antimicrobial activity inhibited
HMW HA 1% + CMC 2% and G3KLcys	128–256	
G3KLcys covalent grafting:		
HMW HA 1% + CMC 2% and G3KLcys-DAH-CMTMC	2–8	G3KLcys antimicrobial activity preserved
G3KLcys-DAH-CMTMC to CS (ratio 5:1) nanoparticles	33	Slight inhibition of antimicrobial activity due to charge competition

[a] TC: tested concentrations for HMW HA 1% + CMC 2%. MIC is expressed as the μg equivalent of AMPD in the conjugate composition calculated based on the degree of substitution obtained from AAA (Table S1). The stars represent different levels of synergy of the conjugate with respect to G3KLcys and chitosan derivatives (very strong synergy (*****); strong synergy (****) and synergy (***)) calculated using the fractional inhibitory index (FIC) based on the Chou-Talalay method (Chou, 2006) (calculations shown in Table S1).

both CMC and CMTMC was calculated (Fig. 1; Table S1). The solubility of the final obtained conjugates was another important parameter for choosing the best crosslinker. Based on the MIC values, solubility, and degree of substitution, sulfo-SIAB was selected for further studies for coupling G3KLcys to CMTMC (G3KLcys-DAH-CMTMC), while sulfo-GMBS was selected for CMC conjugates (G3KLcys-DAH-CMC).

Moreover, the minimal bactericidal concentration (MBC) was measured for these two selected agents (Table S1). The killing efficiency of both G3KLcys-DAH-CMTMC and G3KLcys-DAH-CMC against *P. aeruginosa* was >99.99% at 2 × MIC (4-log reduction). These results showed strong bactericidal activity of the AMPD conjugates against *P. aeruginosa*. Overall, the *in vitro* data support the high activity of the AMPD conjugates against *P. aeruginosa*.

In general, coupling AMPDs to CMTMC leads to slightly higher activity than with CMC derivatives. This may outline the contribution of cationic charges to the synergistic effect. However, this does not suffice to explain the enhancement seen upon CMC coupling. The data show that for both polymers, the activity of the AMPD is preserved and even enhanced through covalent coupling. This difference in antimicrobial activity might be attributed to the enhanced membrane translocation of the conjugates and/or stronger interaction between AMPD conjugates and cytoplasmic components promoted by a better presentation to the cells.

3.3. ^{1}H NMR and FTIR characterization

^{1}H NMR data confirmed the presence of chemical shifts characteristic for different coupling steps (Fig. 2), mentioned previously (Patrulea et al., 2016). Specifically, chemical shifts for chitosan were assigned at δ = 3.87 ppm (s, 2H), 3.70 (s, 4H), 3.13 (s, 1H), 2.01 (s, 0H); for TMC: δ 5.50–4.91 (m, 1H), 3.33 (d, J = 17.8 Hz, 3H, trimethyl units), 3.03 (s, 4H, dimethyl units), 2.03 (s, 1H); for CMTMC: δ 5.5–5.0 (m, 1H), 4.37–4.2 (d, m, -CH2-COOH), 3.28 (d, J = 6.5 Hz, trimethyl units –$(CH_3)_3^+$), 3.01 (s, dimethyl units –$(CH_3)_2$), 2.01 (s, 1H); for DAH-

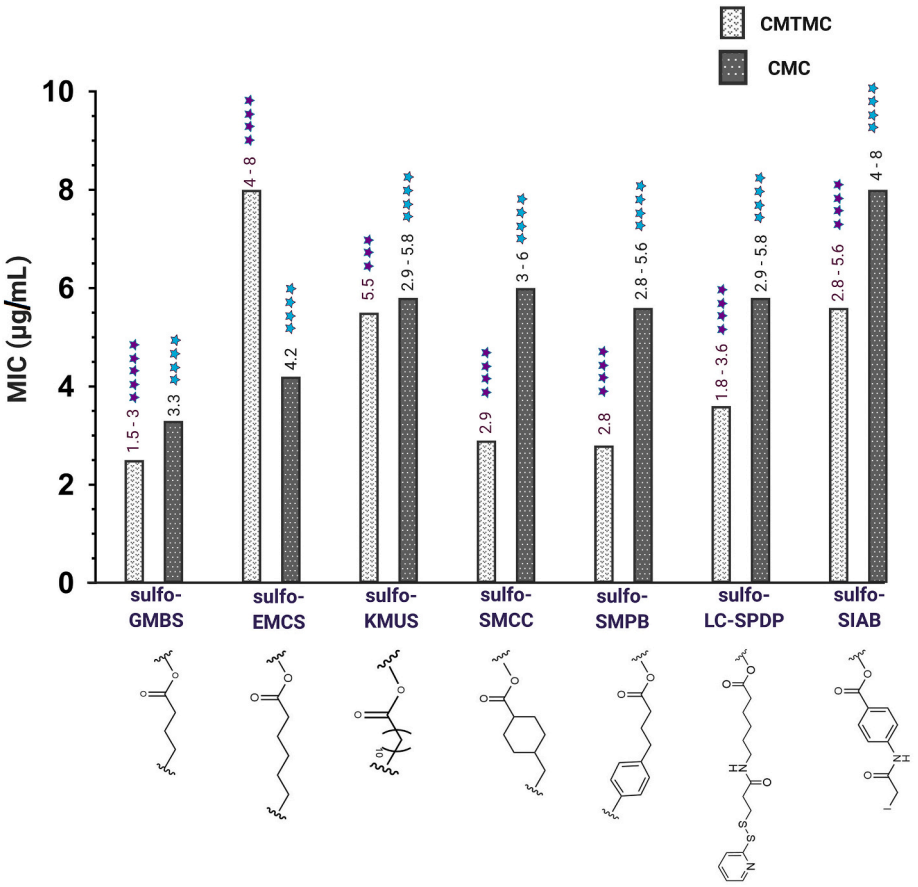

Fig. 1. Antimicrobial activity (MIC) against *P. aeruginosa* and levels of synergy (shown with stars) for both CMTMC and CMC derivatives coupled to G3KLcys *via* 7 sulfo-crosslinkers (sulfo-GMBS; sulfo-EMCS; sulfo-KMUS; sulfo-SMCC; sulfo-SMPB; sulfo-LC-SPDP and sulfo-SIAB). Sulfo-crosslinkers have *N*-hydroxy-succinimide esters and maleimide or other reactive groups in their composition (see full structures in Fig. S1).

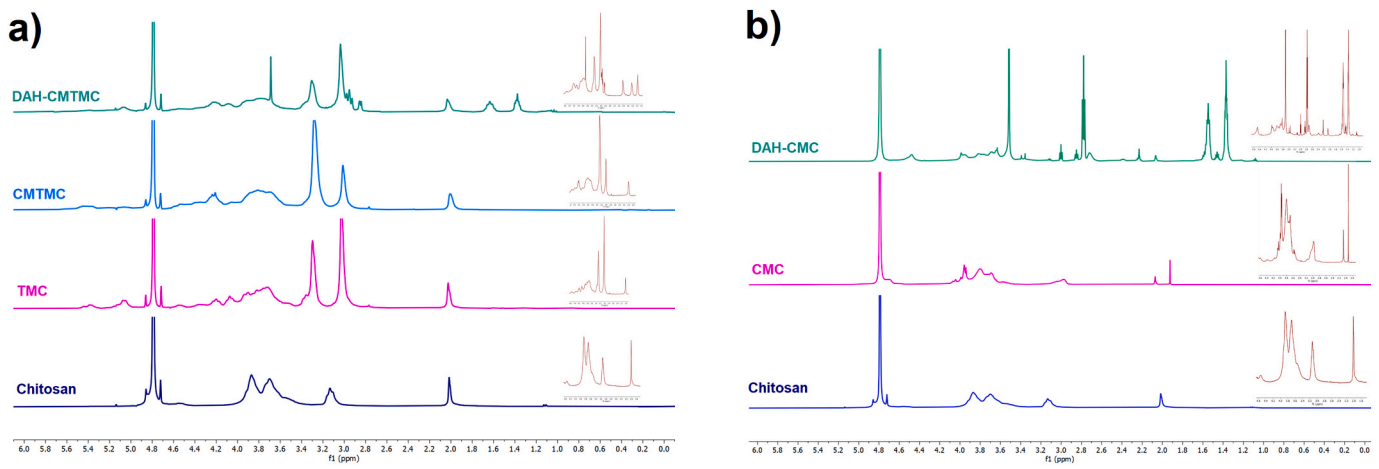

Fig. 2. ^{1}H NMR spectra (600 MHz, D_2O, 22 °C) for a) chemical shifts present during the synthesis of DAH-CMTMC starting with chitosan; TMC; CMTMC; DAH-CMTMC and b) DAH-CMC starting with chitosan; CMC and DAH-CMC.

CMTMC: δ 3.69 (s, -CH_2 in the neighborhood of –NH–), 2.96 (s, -CH_2 from the -NH_2 neighborhood), 2.03 (s, 1H, acetyl groups), 1.64 (s, symmetric and asymmetric –CH_2 groups from DAH spacer), 1.37 (s, -NH_2 at the end of the spacer arm); for CMC: δ 4.04 and 3.96 (s, -CH_2COOH at C-3 and C-6), 2.98 (s, 4H), 2.07 (s, 1H), 1.92 (s, 1H); and for DAH-CMC: δ 3.52 (s, -CH_2 in the neighborhood of –NH–), 2.78 (s,

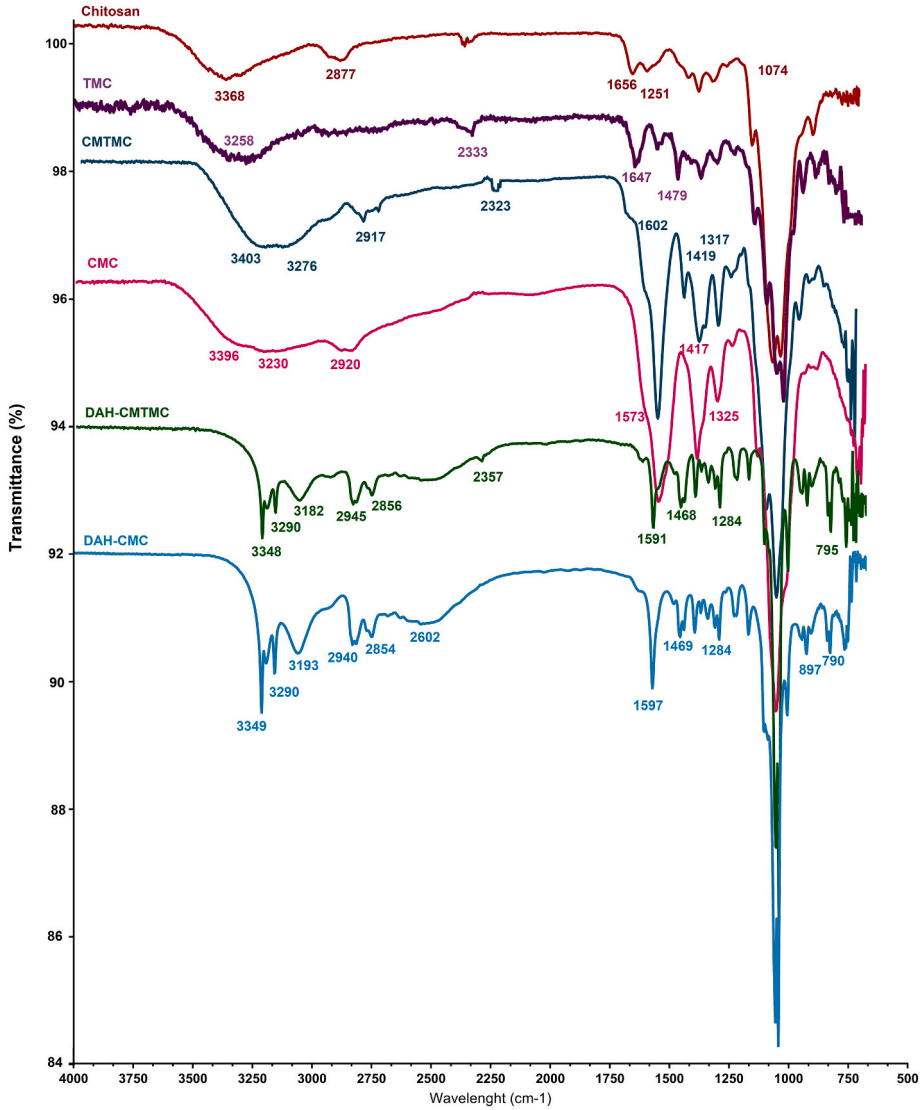

Fig. 3. FTIR spectra for chitosan; TMC; CMTMC; CMC; DAH-CMC and DAH-CMC.

-CH_2 in the neighborhood of –NH–), 1.55 (s, symmetric and asymmetric –CH_2 groups from DAH spacer), 1.37 (s, -NH_2 at the end of the spacer arm).

After each reaction step, FTIR spectra were run and confirmed the presence of the characteristic peaks in chitosan and its derivatives (Fig. 3), as previously mentioned (Patrulea et al., 2016). The bands present in chitosan backbone at 3368; 2877; 1656; 1251 and 1074 cm^{-1} correspond to O—H and N—H; CH_2; —$NHCOCH_3$ and C═O stretching, respectively. For TMC, the most important band is at 2333 cm^{-1}, corresponding to trimethyl groups. In CMTMC, the presence of carboxymethyl groups can be observed at 1602; 1419 and 1317 cm^{-1}, while in CMC at 1573; 1417 and 1325 cm^{-1}. Characteristic peaks present in DAH-CMTMC and DAH-CMC are at 3348; 3290 and 3182 cm-1, corresponding to symmetric and asymmetric NH_2, while bands at 1591; 1468 and 1284 cm^{-1} belong to N—H stretching. This confirms successful spacer addition as shown by ^{1}H NMR as well.

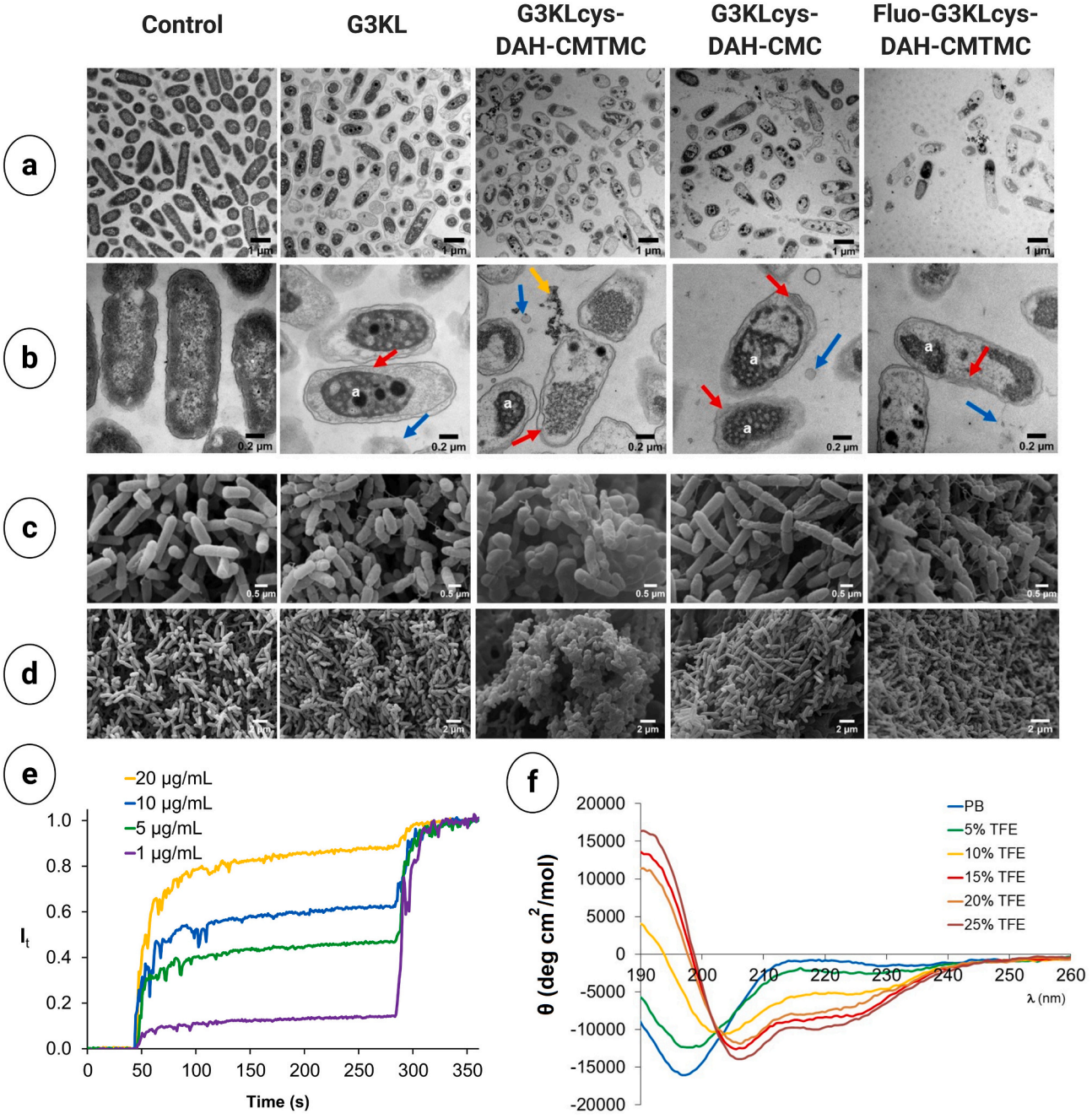

Fig. 4. Assessment of the bacterial killing mechanism of the antimicrobial agents. TEM (a, b) and SEM (c, d) images of 10^9 CFU/mL of *P. aeruginosa* exposed to antimicrobial agents. Treatment conditions: All bacteria were exposed to 40 µg/mL concentrations of antimicrobial conjugates (G3KL, G3KLcys-DAH-CMTMC; G3KLcys-DAH-CMC and Fluo-G3KLcys-DAH-CMTMC) for 60 min in M63 minimal medium. Control: *P. aeruginosa* with no treatment. The arrows for TEM images represent damage caused to *P. aeruginosa*: red: inner membrane disruption; blue: cell debris, vesicle-like structures from the outer membrane disruption; yellow: leakage of the cell content; and a: aggregation of cellular content (compound and DNA/protein). e) Fluorescein leakage assay from PG lipid vesicles. Lipid vesicles were suspended in buffer (10 mM TRIS, 107 mM NaCl, pH 7.4). After 50 s, G3KL-DAH-CMTMC was added to reach the indicated concentration in the lipid vesicle solution. After 250 s, 1.2% Triton X-100 was added for the full release of fluorescein. f) CD spectra of G3KLcys-DAH-CMTMC (200 mg/mL) in phosphate buffer (PBS: 8.0 mM, pH 7.4) upon the addition of TFE (more details are presented in Fig. S6 and S7).

3.4. G3KLcys-chitosan conjugates disrupt the bacterial membrane

The integrity of the bacterial membrane was investigated using different techniques to understand the interactions between selected AMPD conjugates and bacteria (Fig. 4). The exposure of *P. aeruginosa* at 2 × MIC of AMPD-chitosan conjugates for 60 min affected a large bacterial population. Similar behavior was confirmed by transmission electron microscopy (TEM) (Fig. 4a, b). Bacterial cells exposed to G3KLcys-chitosan conjugates showed extensive disruption at both the inner and outer bacterial membranes; leakage and aggregation of cellular content could be observed by TEM. Morphological changes in *P. aeruginosa* were also observed using SEM before and after the addition of antimicrobial agents (Fig. 4c, d). These results suggest that AMPD-chitosan conjugates are membrane-disruptive compounds similar to native G3KL AMPD (Gan et al., 2019).

The membrane disruptive activity of the G3KLcys-chitosan conjugates was further evidenced by vesicle leakage experiments using large unilamellar vesicles (LUVs). LUVs consisting of an anionic lipid, phosphatidyl glycerol (PG), which mimics the bacterial membrane, were loaded with fluorescein. Upon treatment with the conjugates, LUVs released fluorescein, which evidenced membrane perturbation. In contrast, no effect was observed on fluorescein-loaded zwitterionic phosphatidyl ethanolamine (PE) vesicles that mimic eukaryotic cell membranes (Fig. 4e and Fig. S6).

Taking the results together, SEM and TEM imaging and vesicle leakage experiments outline a similar mechanism of action for G3KL and G3KLcys-chitosan conjugates. Furthermore, the circular dichroism (CD) spectrum of the covalently coupled conjugates showed preserved features of a G3KL secondary structure, with a random coil signal in neutral aqueous buffer and an α-helix structure in the presence of 20% trifluoroethanol (TFE) (Fig. 4f and Fig. S7). Overall, these data suggest that AMPD linked to chitosan derivatives leads to fast bacterial killing while maintaining AMPD activity.

3.5. The time-lapse assay indicates that G3KLcys-DAH-CMTMC enters rapidly into P. aeruginosa

As observed by TEM and SEM imaging (Fig. 4a-d), G3KLcys-chitosan conjugates severely disrupt both inner and outer bacterial membranes. We next tracked the transport of the conjugate in *P. aeruginosa* over time using confocal time-lapse imaging. Bacterial cells (10^9 CFU/mL) were incubated with Fluo-G3KLcys-DAH-CMTMC (fig. S3) at 40 μg/mL (equivalent to 2 × MIC) in the presence of propidium iodide (PI), a fluorescent dye that binds to DNA once bacteria are permeabilized. For live imaging, bacterial cells were trapped inside an M63 agarose pad, followed by PI addition, the start of recording, and Fluo-AMPD-conjugate addition (Gan et al., 2019; Schneider et al., 2016). Fluo-G3KLcys-DAH-CMTMC stained the bacterial surface immediately upon addition of the fluorescent conjugate (Fig. 5, Fig. S11, Video S1 and Video S2), whereas PI was detected in the cell after a short delay of 1 min. The fluorescence signal of the conjugates and the PI stayed stable for the next 7 min. At 8–9 min, the signal of the conjugates and PI significantly increased. The results suggested that the conjugates accumulated first at the bacterial surface until significant membrane disruption occurred to enable the entry of the whole conjugate inside the bacterial cell, which is consistent with the accumulation effect observed by TEM imaging (Fig. 4a-d). As bacteria are trapped in agarose pad, we observed a delay in detection of Fluo-G3KLcys-DAH-CMTMC for other bacteria in the movie (Video S2 and Fig. S11), which we believe it is due to diffusion rate of the compound through the pad.

Time-killing kinetics assay confirmed that G3KLcys-DAH-CMTMC efficiently killed *P. aeruginosa* after 30 min at a concentration of 2 × MIC and 4 × MIC compared to the native G3KL (Fig. 6a). These results indicate that bacterial killing activity of G3KL was preserved upon conjugation to chitosan. Moreover, stability assay (Fig. 6b) in human serum showed that native G3KL had a 2-fold increase of MIC at already 6 h, while G3KLcys-DAH-CMTMC showed the same activity after 48 h. These results demonstrate that the activity of G3KL was preserved upon

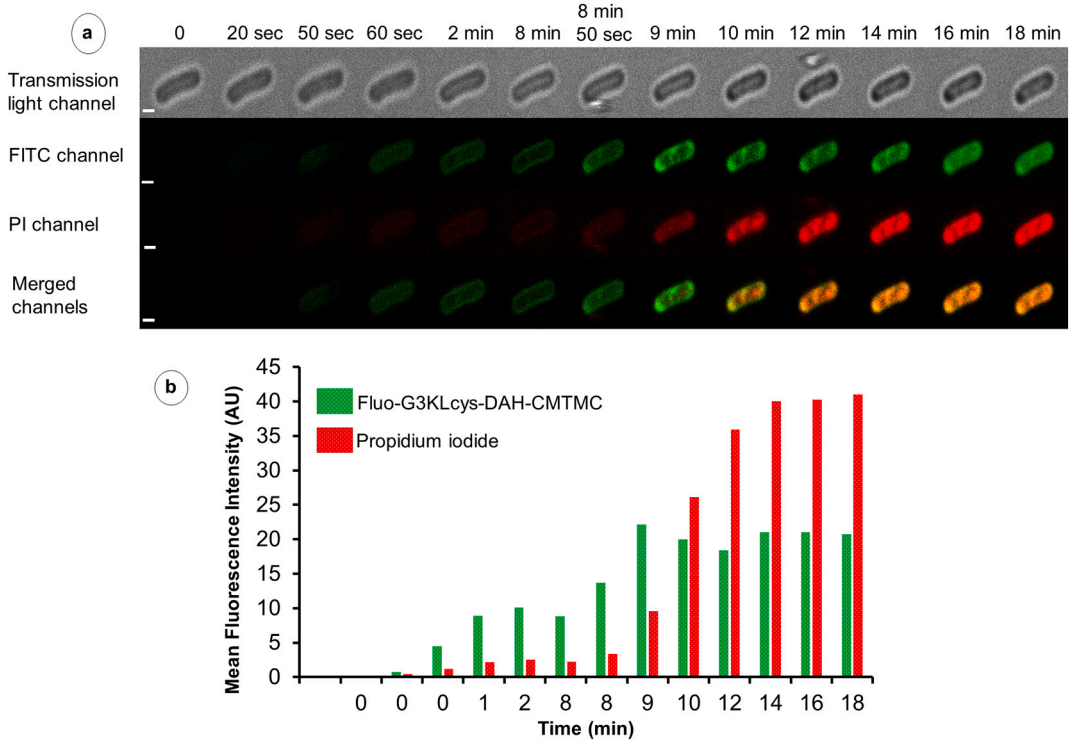

Fig. 5. a) Time-lapse images for tracking the interaction between Fluo-G3KLcys-DAH-CMTMC and *P. aeruginosa* cells. Cells were exposed to a concentration of 2 × MIC and PI. Scale bars are 1 μm. Total uptake of AMPD conjugate and PI was 15 min on average. PI was observed 1–2 min after the appearance of the conjugate and seemed to be gradually taken up. b) Mean fluorescence intensity of Fluo-G3KLcys-DAH-CMTMC and PI extracted using ImageJ.

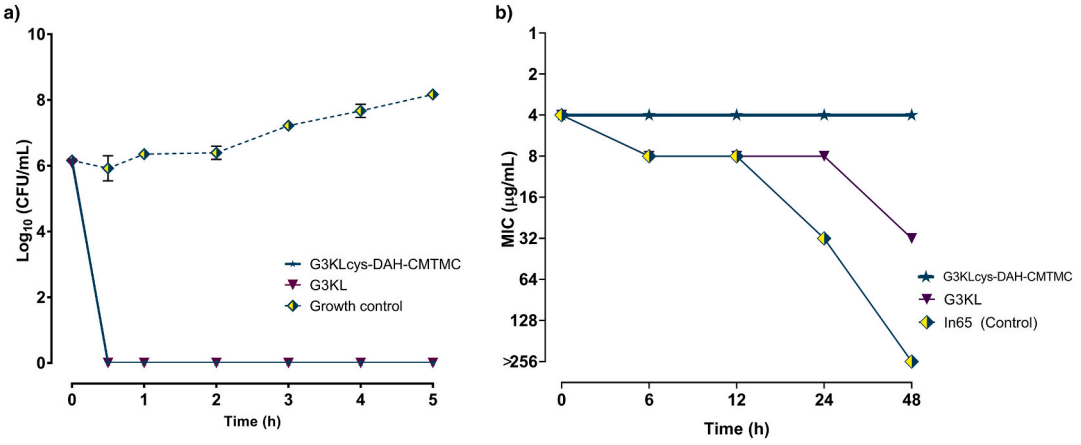

Fig. 6. a) Time-kill kinetics assay of G3KLcys-DAH-CMTMC and G3KL (at 2× initial MIC, or 8 μg/mL) and b) MIC value after incubation with 12.5% human serum. All experiments have been run in triplicates and error bars indicate standard deviation (SD).

coupling, indicating a protective effect of chitosan derivatives. For instance, the linear peptide In65 (Stéphane et al., 2021) (used as a control) had a 2-, 8- and > 64-fold increase of MIC after 6, 12 and 48 h, respectively, suggesting that In65 was partially degraded in human serum after 6 h of incubation. We also observed that G3KLcys-conjugate kept the same antimicrobial activity after storing G3KLcys-DAH-CMTMC in MHB for 6 months at 4 °C (data not shown) and running a MIC assay against *P. aeruginosa*.

Moreover, G3KL and Fluo-G3KL were previously shown to interact with lipopolysaccharides and accumulate in bacterial cells but did not accumulate in mammalian cells (Gan et al., 2019). Since the mechanism of antimicrobial activity of AMPD conjugates was preserved upon coupling to chitosan derivatives, we may expect a similar absence of mammalian cell accumulation for the AMPD-chitosan conjugates.

3.6. Preserved antimicrobial activity of embedded G3KLcys-chitosan derivatives into application-specific formulations

In a clinical setup, bandages are most often used for retaining moisture and protecting wounds from further microbial infection (Abdel-Sayed et al., 2019). As shown in Scheme 2, the simple addition of AMPD to a dressing is not a viable strategy, because it hinders the antimicrobial activity of AMPD. Interestingly, by embedding G3KLcys-chitosan conjugates into HA 1% and CMC 2% matrix, we observed no inhibition of G3KL activity (Table 1). In contrast, the results showed that the biological activity of AMPD incorporated into dressings was preserved only when coupled to chitosan derivatives (MIC: 3.9–7.8 μg/mL). This suggests that chitosan derivatives may confer antimicrobial activity on wound dressing biomaterials.

Additionally, nanoparticles (NPs) may be used to deliver the AMPD to the infected site, either for topical or non-topical applications by spraying. For instance, in open surgery, spraying antimicrobial NPs would facilitate and safely deliver AMPDs to the target site. Therefore, we designed such formulations for the treatment of small and/or infected wounds. NPs were prepared *via* the "one-shot" method by mixing positively charged AMPD-DAH-CMTMC and negatively charged chondroitin sulfate (CS) as previously described in our protocols (Patrulea et al., 2019). Optimized NPs (for details see Fig. S8 and S10) showed MICs not higher than that of the parent peptide, suggesting slight inhibition of the antimicrobial activity, which we attributed to the charge screening effect of CS. In the context of a sprayable formulation, the nanoparticle dose would be adapted to achieve efficient activity at the target site.

3.7. Safety assessment of AMPD-chitosan conjugates: toxicity and hemolysis

A recognized drawback of AMPs/AMPDs is their toxicity towards healthy tissues and their high hemolytic activity towards RBCs (Rončević et al., 2019). Therefore, to evaluate the safety of the AMPD conjugates, the toxicities of both G3KLcys-DAH-CMTMC and G3KLcys-DAH-CMC towards HDFs and mouse RBCs were evaluated. The mitochondrial activity of HDFs was measured after 2 and 4 days in contact with AMPD conjugates (Fig. 7a).

G3KLcys coupled to the CMTMC derivative was slightly more toxic than G3KLcys-DAH-CMC. This is expected due to positive charges arising from the CMTMC derivative. However, the cytotoxicity assay supports the safety of both conjugates for concentrations ranging from 1 to 5 × MIC for AMPD-CMTMC and 1 to 10 × MIC for AMPD-CMC. On the other hand, hemolysis results (Fig. 7b) confirm the safety of both conjugates at doses ranging from 1 to 10 × MIC. The highest hemolysis rate (2.9%) is again observed for positively charged CMTMC, albeit only at 20 × MIC. The toxicity of the AMPD conjugates was significantly decreased upon coupling to chitosan derivatives when compared to native AMPD (**$p < 0.01$ and ****$p < 0.0001$). These results are in line with the lack of membrane-disrupting activity of the conjugates towards PE vesicles mimicking eukaryotic membranes (Fig. 4e). AMPD-chitosan does not hamper membrane development, as suggested by the normal growth of the vasculature observed *ex vivo* using the chick chorioallantoic membrane (CAM) assay, which is an indication of its nontoxicity (Fig. S14). The CAM assay has been approved by FDA for products preclinically evaluated for the treatment of chronic cutaneous ulcers and burn wounds (Ribatti, 2016).

3.8. Assessment of HDF exposed to solubilized biopolymer matrix (gel matrix) incorporating conjugated AMPD

HDFs were treated with both G3KLcys-DAH-CMTMC and G3KLcys-DAH-CMC embedded into CMC 2% and HA 1% dressings (Fig. 8; preparation of the dressings and their characterization detailed in Fig. S9 and S10). Remarkably, in addition to high potency against *P. aeruginosa*, AMPD-chitosan derivatives embedded into HA 1% and CMC 2% matrix were nontoxic to HDF even after 7 days of exposure at 1 × MIC.

Giemsa staining revealed no hindrance to HDF exposed to both AMPD-chitosan derivatives incorporated into CMC 2% and HA 1%, which suggests full biocompatibility with HDF. Such dressings are promising candidates for further *in vivo* studies.

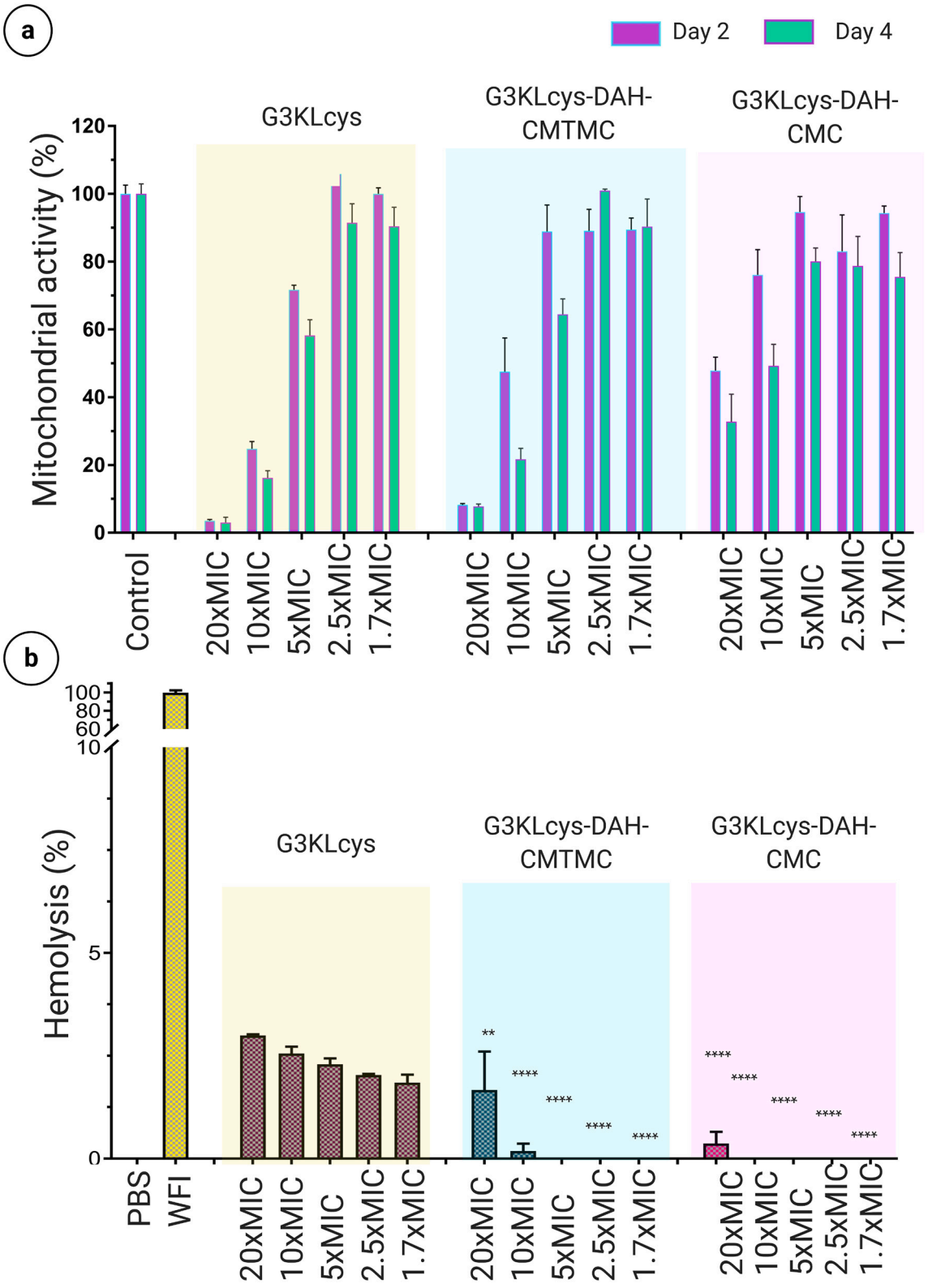

Fig. 7. Toxicity assessment of AMPD-chitosan conjugates against (a) HDF after 2 and 4 days of treatment and (b) RBCs with phosphate-buffered saline (PBS) and water for injection (WFI) as controls. HDFs were seeded at 2×10^5 cells/mL and cultured for 48 h to reach complete confluence. The control group was tissue culture plate (TCP)-treated HDF. Both G3KLcys-DAH-CMTMC and G3KLcys-DAH-CMC were evaluated at different concentrations in DMEM from 1.7 to 20 × MIC. The MIC refers to the concentration of the AMPD in the conjugates. Data from AAA were used to calculate the amount of the peptide coupled to chitosan derivatives. PBS and water for injection (WFI) were considered 0% and 100% lysis, respectively. Hemolysis of the AMPD-chitosan conjugates was significantly reduced compared to AMPD alone. Significant differences over G3KLcys are indicated as $^{**}p < 0.01$ and $^{****}p < 0.0001$ using two-way analysis of variance (ANOVA) and the Sidak test. Error bars represent mean value ± standard error of the mean (SEM; $n = 3$).

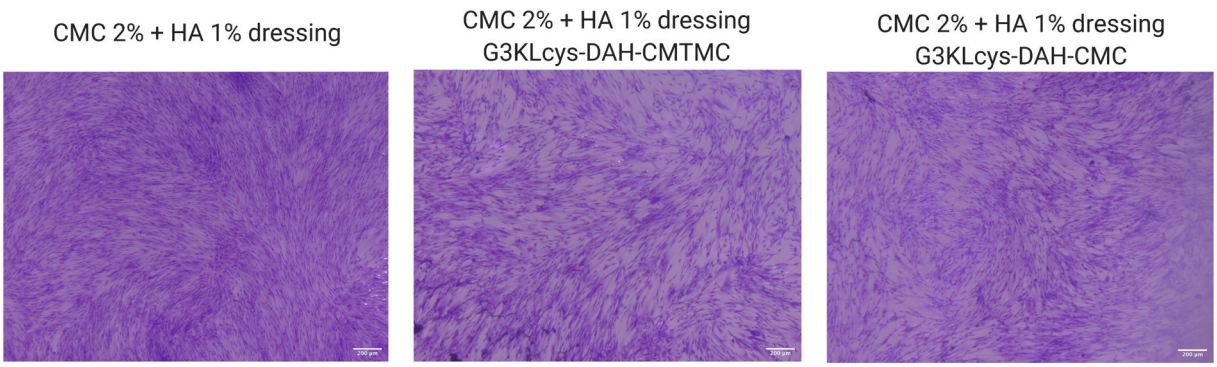

Fig. 8. Giemsa staining of HDF after 7 days of treatment with CMC 2% and HA 1% matrix; G3KLcys-DAH-CMC (1 × MIC) and G3KLcys-DAH-CMTMC (1 × MIC). Progenitor HDFs were seeded in a 6-well plate at a density of 3000 cells/cm^2 on top of 1 × 1 cm^2 bandages (scale bars 200 μm).

3.9. The AMPD-chitosan conjugate is a general strategy for peptide delivery and antimicrobial activity preservation or enhancement

The new technological platform described herein based on CMTMC and CMC chitosan derivatives is not limited to third-generation dendrimer peptides but can be used to couple a broad range of peptides. To illustrate this, linear peptide, and 2nd generation AMPD were coupled to chitosan derivatives, similar to 3rd generation AMPD *via* thiol-maleimide click chemistry using both sulfo-SIAB and sulfo-GMBS crosslinkers.

Synergistic antimicrobial activity against *P. aeruginosa* resulted upon coupling of linear peptide and 2nd generation AMPD to chitosan derivatives. The degree of synergy between AMPDs and both CMC and CMTMC was calculated using the Chou-Talalay method (Chou, 2006) (Table 2 and Table S2).

Coupling of linear peptide to CMTMC leads to stronger synergy, while coupling the linear peptide to CMC leads to lower synergy. This might be attributed to positive charges arising from the CMTMC derivative, which act synergistically with AMPDs. However, this sole charge does not account for G2KL, which shows higher synergy with CMC, probably due to additional interactions such as hydrophobic interactions or steric hindrance. Coupling linear AMP to chitosan derivatives *via* both crosslinkers led to synergistic antimicrobial effects between the two compounds. For the linear peptide, coupling *via* sulfo-SIAB resulted in higher synergy, while for the 2nd generation AMPD, using sulfo-GMBS crosslinker led to slightly better synergy. Therefore, another factor that could influence the synergy is the length and ramification of the AMPDs, which would affect their steric hindrance.

Importantly, conjugation with chitosan derivatives can be carried out with both linear peptide and 2nd generation AMPD without altering their antibacterial activity. In contrast, the antimicrobial activity against *P. aeruginosa* was enhanced after coupling to both CMTMC and CMC. For instance, Li et al. coupled a third-generation poly(amidoamine) (PAMAM-G3), a polymer-based dendrimer, to chitosan using copper-catalyzed azide-alkyne reaction of azide-modified chitosan (Li et al., 2018). The PAMAM-G3-chitosan significantly inhibited the growth of Gram-negative *E. coli* and Gram-positive *S. aureus* at micromolar scale range using zone of inhibition assay. However, the mechanism is not fully elucidated. Sahariah et al. attached covalently anoplin, a linear AMP, to different chitosan derivatives *via* copper-catalyzed alkyne–azide coupling chemistry (Sahariah et al., 2015). However, the MIC against *P. aeruginosa* was high, in the range of 18–148 μg/mL, though the coupling led to an enhanced antibacterial activity and absence of hemolysis compared to parent peptide. Moreover, strategies to deliver AMPs against bacterial infections have been detailed in different reviews (Kawano et al., 2020; Nordström & Malmsten, 2017; Patrulea et al., 2020).

Table 2
MIC (μg/mL) and synergy calculated based on the Chou-Talalay method for 1st- and 2nd-generation AMPDs coupled to chitosan derivatives *via* sulfo-SIAB and sulfo-GMBS crosslinkers against *P. aeruginosa.*

AMPD	Chitosan derivative	Crosslinker	MIC (μg/mL)	Synergy level[a]
SB1cys	–	–	16	
SB1cys	DAH-CMTMC	sulfo-SIAB	4.1–8.2	****
	DAH-CMC		13.8	*
	DAH-CMTMC	sulfo-GMBS	8.0	***
	DAH-CMC		7.5	***
G2KLcys	–	–	128	
G2KLcys	DAH-CMTMC	sulfo-SIAB	80.6	**
	DAH-CMC		28.9	****
	DAH-CMTMC	Sulfo-GMBS	>83.5	*
	DAH-CMC		10.7	*****
	CMTMC[b]	–	No activity	–
	CMC[b]	–	No activity	–

[a] Synergy scale: "*****" = very strong synergy "****" = strong synergy; "***" = synergy; "**" = moderate synergy; "*" = slight synergy.
[b] CMTMC and CMC derivatives were tested at a concentration of 2048 μg/mL.

3.10. G2KLcys- and SB1cys-conjugates disrupt the membrane of P. aeruginosa

Upon treatment with the linear peptide and G2KLcys-chitosan conjugates, PG released fluorescein, indicating a membrane-disruptive activity of the compounds. Interestingly, SB1cys was able to induce the release of fluorescein loaded in zwitterionic PE vesicles that mimic eukaryotic cell membranes (Fig. S6), whereas the fluorescein level was reduced with SB1cys-chitosan, which could be consistent with the toxicity results. We hypothesize that chitosan can reduce the toxicity of the linear peptide in mammalian cells. The PE membrane was weakly affected by G2KLcys and G2KLcys-chitosan, which suggests moderate hemolytic activity and toxicity in mammalian cells.

The anionic PG vesicle assay showed that the bacterial membranes were perturbed by the addition of both SB1cys-DAH-CMTMC and G2KLcys-DAH-CMTMC in the same manner as the native AMPD (Fig. S6). However, a change in spectra could be observed on PE, which could indicate mammalian cell toxicity.

3.11. Circular dichroism for G2KLcys- and SB1cys-conjugates

Linear AMPs often undergo a conformational transition upon contact with the bacterial membrane, resulting in a membrane-disruptive amphiphilic structure that is most often observed as an α-helix by CD in aqueous buffer upon the addition of 20% *v*/v TFE (Cotter et al., 2013; Zasloff, 2002). Previous studies showed that SB1 (Baeriswyl et al., 2019) and G2KL (Siriwardena, Stach, et al., 2018b) to a lower extent transit to an α-helical signal upon the addition of 20% v/v TFE. Here, we found that both cys analogs of G2KL and SB1 (G2KLcys and SB1cys), as well as their respective chitosan conjugates, can maintain their secondary

structure in the presence of TFE. More interestingly, the SB1cys-DAH-CMC conjugate adopted an α-helical signal (Fig. S7) in aqueous buffer in line with the antimicrobial efficacy, where the conjugate displayed better activity and stronger synergy between the peptide and chitosan.

3.12. Safety assessment of the G2KLcys- and SB1cys-conjugates using the WST-1 assay

Viability of HDF as assessed by their mitochondrial activity and hemolysis assays indicated that G2KLcys-conjugates are less toxic than linear SB1cys-conjugates (Fig. S12 and S13). Specifically, at day 2, the 2nd generation dendrimer conjugates exhibited viabilities higher than 80% compared to the healthy control, up to a high concentration of the antimicrobial compound - 10 × MIC. SB1cys-DAH-CMC exhibited high (>80%) cell viability up to 5 × MIC at day 2, in contrast to the corresponding CMTMC conjugate, which demonstrated poor viability at 2.5 × MIC. This is expected mainly due to the positive charges of the cationic CMTMC. These data confirm the potential of chitosan derivative conjugation for dendrimers and selected linear antimicrobial peptides.

4. Conclusions

In this study, we have demonstrated for the first time that conjugation to chitosan derivatives is a suitable chemical platform for attaching different antimicrobial peptide dendrimers with enhanced biological activity against pathogens, such as Gram-negative *P. aeruginosa*. This is an important advance, as these peptides, which are very effective against MDR bacteria, represent an alternative to antibiotics in wound dressings but are unstable for longer than 24 h. Chemical grafting of AMPDs to the biopolymer derivatives used herein reduced toxicity towards mammalian cells while maintaining high antibacterial activity. The fluorescently labeled G3KLcys-chitosan conjugate bearing fluorescein revealed the internalization and accumulation of the conjugate into the bacteria after disruption of the outer and inner membrane using time-lapse confocal microscopy.

Moreover, the new chemistry proved to be efficient not only to preserve AMPD bioactivity but also to allow synergistic antimicrobial effects of the conjugates. Whereas AMPDs alone mixed into biopolymer matrices lost their activity, G3KLcys-conjugates incorporated into wound dressings preserved the activity of the native AMPD. The decreased hemolytic activity is a further important aspect to consider when designing a new antimicrobial system to balance biological efficacy *versus* toxicity to mammalian cells.

One of the purposes of this new conjugation approach was to design unique foam-like dressings containing an active biopolymer, which can be easily applied and adapted to the shape of the wound and will bear antibacterial bioactive AMPDs. The known ability of the chitosan/HA biopolymer dressings to promote wound healing would be a key asset for infected wound treatment. Additionally, sprayable nanoparticles for small surgical wounds could be easily applied at the site of the injury. The incorporation of AMPD conjugates into nanocomplexes could further protect the active principle from the enzymatic degradation usually occurring in wound exudates. This unique chemical platform may allow the introduction of AMPDs into the therapy of chronic wounds.

Supplementary data to this article can be found online at https://doi.org/10.1016/j.carbpol.2021.119025.

CRediT authorship contribution statement

Viorica Patrulea: Conceptualization, Methodology, Validation, Formal analysis, Investigation, Data curation, Writing – original draft, Writing – review & editing, Visualization, Funding acquisition, Supervision, Project administration. **Bee-Ha Gan:** Methodology, Validation, Formal analysis, Investigation, Data curation, Writing – review & editing, Visualization. **Karl Perron:** Methodology, Validation, Formal analysis, Investigation, Data curation, Writing – review & editing, Visualization. **Xingguang Cai:** Methodology, Validation, Investigation, Data curation, Writing – review & editing. **Philippe Abdel-Sayed:** Methodology, Validation, Investigation, Data curation, Writing – review & editing. **Emmanuelle Sublet:** Methodology, Validation, Formal analysis, Writing – review & editing. **Verena Ducret:** Methodology, Validation, Formal analysis, Writing – review & editing. **Natalia Porroche Nerhot:** Methodology, Formal analysis, Investigation, Writing – review & editing. **Lee Ann Applegate:** Validation, Data curation, Writing – review & editing, Visualization. **Gerrit Borchard:** Conceptualization, Validation, Writing – review & editing. **Jean-Louis Reymond:** Conceptualization, Validation, Writing – review & editing, Visualization, Supervision. **Olivier Jordan:** Conceptualization, Methodology, Validation, Writing – review & editing, Visualization, Funding acquisition, Supervision, Project administration.

Declaration of competing interest

The authors declare the following financial interests which may be considered as potential competing interests: V. Patrulea, O. Jordan, B. Ha Gan, G. Borchard and J.-L. Reymond are co-inventors of a patent #WO2020225255A1 “Antimicrobial tailored chitosan” pending to University of Geneva and University of Bern.

Acknowledgment

This work was supported by an Innogap fund by the Unitec office of the University of Geneva (Technologie 1037-A985). Dr. Viorica Patrulea is a recipient of the Swiss National Science Foundation grant (project ID: P400PM_194482). We thank Dr. Laurence Marcourt (University of Geneva) for running the NMR spectra. We also thank Analytical Research and Services (University of Bern, Switzerland) for running the amino acid analysis. Primex (Iceland) is acknowledged for the kind donation of chitosan. Electron microscopy sample preparation and imaging were performed with devices supported by Mr. Beat Haenni from the Microscopy Imaging Center of the University of Bern, Switzerland.

References

Abdel-Sayed, P., Hirt-Burri, N., de Buys Roessingh, A., Raffoul, W., & Applegate, L. A. (2019). Evolution of biological bandages as first cover for burn patients. *Advances in Wound Care, 8*(11), 555–564.

Abdel-Sayed, P., Kaeppli, A., Siriwardena, T., Darbre, T., Perron, K., Jafari, P., Reymond, J.-L., Pioletti, D. P., & Applegate, L. A. (2016). Anti-microbial dendrimers against multidrug-resistant P. aeruginosa enhance the angiogenic effect of biological burn-wound bandages. *Scientific Reports, 6*(1), 22020.

Baeriswyl, S., Gan, B.-H., Siriwardena, T. N., Visini, R., Robadey, M., Javor, S., Stocker, A., Darbre, T., & Reymond, J.-L. (2019). X-ray crystal structures of short antimicrobial peptides as Pseudomonas aeruginosa lectin B complexes. *ACS Chemical Biology, 14*(4), 758–766.

Belbekhouche, S., Guerrouache, M., & Carbonnier, B. (2016). Thiol-maleimide Michael addition click reaction: A new route to surface modification of porous polymeric monolith. *Macromolecular Chemistry and Physics, 217*(8), 997–1006.

Caires, R. A., da Costa e Silva, V. T., Burdmann, E. A., Coelho, F. O., & Costalonga, E. C. (2019). Drug-induced acute kidney injury. In C. Ronco, R. Bellomo, J. A. Kellum, & Z. Ricci (Eds.), *Critical care nephrology* (3rd ed., pp. 214–221). Philadelphia: Elsevier. e212.

Chen, C. H., & Lu, T. K. (2020). Development and challenges of antimicrobial peptides for therapeutic applications. *Antibiotics, 9*(1), 24.

Chin, W., Zhong, G., Pu, Q., Yang, C., Lou, W., De Sessions, P. F., Periaswamy, B., Lee, A., Liang, Z. C., Ding, X., Gao, S., Chu, C. W., Bianco, S., Bao, C., Tong, Y. W., Fan, W., Wu, M., Hedrick, J. L., & Yang, Y. Y. (2018). A macromolecular approach to eradicate multidrug resistant bacterial infections while mitigating drug resistance onset. *Nature Communications, 9*(1), 917.

Chou, T.-C. (2006). Theoretical basis, experimental design, and computerized simulation of synergism and antagonism in drug combination studies. *Pharmacological Reviews, 58*(3), 621–681.

Costa, F., Carvalho, I. F., Montelaro, R. C., Gomes, P., & Martins, M. C. L. (2011). Covalent immobilization of antimicrobial peptides (AMPs) onto biomaterial surfaces. *Acta Biomaterialia, 7*(4), 1431–1440.

Cotter, P. D., Ross, R. P., & Hill, C. (2013). Bacteriocins — A viable alternative to Antibiotics? *Nature Reviews Microbiology, 11*(2), 95–105.

de la Cruz-Hernández, I., Cornejo-Juárez, P., Tellez-Miranda, O., Barrera-Pérez, L., Sandoval-Hernández, S., Vilar-Compte, D., Velázquez-Acosta, C., & Volkow, P.

(2020). Microbiology and prevalence of E2SKAPE-resistant strains in catheter-related bloodstream infections in patients with cancer. *American Journal of Infection Control, 48*(1), 40–45.
Drayton, M., Kizhakkedathu, J. N., & Straus, S. K. (2020). Towards robust delivery of antimicrobial peptides to combat bacterial resistance. *Molecules, 25*(13), 3048.
Eloff, J. N. (1998). A sensitive and quick microplate method to determine the minimal inhibitory concentration of plant extracts for bacteria. *Planta Medica, 64*(8), 711–713.
Gan, B. H., Gaynord, J., Rowe, S. M., Deingruber, T., & Spring, D. R. (2021). The multifaceted nature of antimicrobial peptides: current synthetic chemistry approaches and future directions. *Chemical Society Reviews, 50*, 7820–7880. https://doi.org/10.1039/D0CS00729C
Gan, B.-H., Siriwardena, T. N., Javor, S., Darbre, T., & Reymond, J.-L. (2019). Fluorescence imaging of bacterial killing by antimicrobial peptide dendrimer G3KL. *ACS Infectious Diseases, 5*(12), 2164–2173.
González-Fernández, E., Staderini, M., Avlonitis, N., Murray, A. F., Mount, A. R., & Bradley, M. (2018). Effect of spacer length on the performance of peptide-based electrochemical biosensors for protease detection. *Sensors and Actuators B: Chemical, 255*, 3040–3046.
Kambhampati, S., Li, J., Evans, B. S., & Allen, D. K. (2019). Accurate and efficient amino acid analysis for protein quantification using hydrophilic interaction chromatography coupled tandem mass spectrometry. *Plant Methods, 15*, 46.
Kawano, Y., Jordan, O., Hanawa, T., Borchard, G., & Patrulea, V. (2020). Are antimicrobial peptide dendrimers an escape from ESKAPE? *Advances in Wound Care, 9*(7), 378–395.
Krishnamurthy, M., Lemmon, M. M., Falcinelli, E. M., Sandy, R. A., Dootz, J. N., Mott, T. M., Rajamani, S., Schaecher, K. E., Duplantier, A. J., & Panchal, R. G. (2019). Enhancing the antibacterial activity of polymyxins using a nonantibiotic drug. *Infection and Drug Resistance, 12*, 1393–1405.
Li, G., Yu, S., Xue, W., Ma, D., & Zhang, W. (2018). Chitosan-graft-PAMAM loading nitric oxide for efficient antibacterial application. *Chemical Engineering Journal, 347*, 923–931.
Mahlapuu, M., Björn, C., & Ekblom, J. (2020). Antimicrobial peptides as therapeutic agents: Opportunities and challenges. *Critical Reviews in Biotechnology, 40*(7), 978–992.
Mulani, M. S., Kamble, E. E., Kumkar, S. N., Tawre, M. S., & Pardesi, K. R. (2019). Emerging strategies to combat ESKAPE pathogens in the era of antimicrobial resistance: A review. *Frontiers in Microbiology, 10*, 539.
Nordström, R., & Malmsten, M. (2017). Delivery Systems for Antimicrobial Peptides. *Advances in Colloid and Interface Science, 242*, 17–34.
Patrulea, V., Applegate, L. A., Ostafe, V., Jordan, O., & Borchard, G. (2015). Optimized synthesis of O-carboxymethyl-N, N, N-trimethyl chitosan. *Carbohydrate Polymers, 122*, 46–52.
Patrulea, V., Borchard, G., & Jordan, O. (2020). An update on antimicrobial peptides (AMPs) and their delivery strategies for wound infections. *Pharmaceutics, 12*(9), 840.
Patrulea, V., Hirt-Burri, N., Jeannerat, A., Applegate, L. A., Ostafe, V., Jordan, O., & Borchard, G. (2016). Peptide-decorated chitosan derivatives enhance fibroblast adhesion and proliferation in wound healing. *Carbohydrate Polymers, 142*, 114–123.
Patrulea, V., Laurent-Applegate, L. A., Ostafe, V., Borchard, G., & Jordan, O. (2019). Polyelectrolyte nanocomplexes based on chitosan derivatives for wound healing application. *European Journal of Pharmaceutics and Biopharmaceutics, 140*, 100–108.
Patrulea, V., Ostafe, V., Borchard, G., & Jordan, O. (2015). Chitosan as a starting material for wound healing applications. *European Journal of Pharmaceutics and Biopharmaceutics, 97*, 417–426.
Ribatti, D. (2016). The chick embryo chorioallantoic membrane (CAM). A multifaceted experimental model. *Mechanisms of Development, 141*, 70–77.
Ronč̆ević, T., Puizina, J., & Tossi, A. (2019). Antimicrobial peptides as anti-infective agents in pre-post-antibiotic era? *International Journal of Molecular Sciences, 20*(22), 5713.
Sahariah, P., Sørensen, K. K., Hjálmarsdóttir, M.Á., Sigurjónsson, Ó. E., Jensen, K. J., Másson, M., & Thygesen, M. B. (2015). Antimicrobial peptide shows enhanced activity and reduced toxicity upon grafting to chitosan polymers. *Chemical Communications, 51*(58), 11611–11614.
Schneider, V. A. F., Coorens, M., Ordonez, S. R., Tjeerdsma-van Bokhoven, J. L. M., Posthuma, G., van Dijk, A., Haagsman, H. P., & Veldhuizen, E. J. A. (2016). Imaging the antimicrobial mechanism(s) of cathelicidin-2. *Scientific Reports, 6*, 32948.
Siriwardena, T. N., Capecchi, A., Gan, B.-H., Jin, X., He, R., Wei, D., Ma, L., Köhler, T., van Delden, C., Javor, S., & Reymond, J.-L. (2018). Optimizing antimicrobial peptide dendrimers in chemical space. *Angewandte Chemie International Edition, 57*(28), 8483–8487.
Siriwardena, T. N., Stach, M., He, R., Gan, B.-H., Javor, S., Heitz, M., Ma, L., Cai, X., Chen, P., Wei, D., Li, H., Ma, J., Köhler, T., van Delden, C., Darbre, T., & Reymond, J.-L. (2018). Lipidated peptide dendrimers killing multidrug-resistant bacteria. *Journal of the American Chemical Society, 140*(1), 423–432.
Stach, M., Siriwardena, T. N., Köhler, T., van Delden, C., Darbre, T., & Reymond, J.-L. (2014). Combining topology and sequence Design for the Discovery of potent antimicrobial peptide dendrimers against multidrug-resistant Pseudomonas aeruginosa. *Angewandte Chemie International Edition, 53*(47), 12827–12831.
Stéphane, B., Hippolyte, P., Ivan, D. B., Thilo, K., Christian, V. D., Achim, S., Sacha, J., & Jean-Louis, R. (2021). Mixed chirality α-helix in a stapled bicyclic and a linear antimicrobial peptide revealed by X-ray crystallography. *ChemRxiv*, 1.
Teixeira, M. C., Carbone, C., Sousa, M. C., Espina, M., Garcia, M. L., Sanchez-Lopez, E., & Souto, E. B. (2020). Nanomedicines for the delivery of antimicrobial peptides (AMPs). *Nanomaterials, 10*(3), 560.
Thapa, R. K., Diep, D. B., & Tønnesen, H. H. (2020). Topical antimicrobial peptide formulations for wound healing: Current developments and future prospects. *Acta Biomaterialia, 103*, 52–67.
Wiegand, I., Hilpert, K., & Hancock, R. E. (2008). Agar and broth dilution methods to determine the minimal inhibitory concentration (MIC) of antimicrobial substances. *Nature Protocols, 3*(2), 163–175.
Wieland, K., Chhatwal, P., & Vonberg, R.-P. (2018). Nosocomial outbreaks caused by Acinetobacter baumannii and Pseudomonas aeruginosa: Results of a systematic review. *American Journal of Infection Control, 46*(6), 643–648.
Xu, L., Shao, C., Li, G., Shan, A., Chou, S., Wang, J., Ma, Q., & Dong, N. (2020). Conversion of broad-spectrum antimicrobial peptides into species-specific antimicrobials capable of precisely targeting pathogenic bacteria. *Scientific Reports, 10*(1), 944.
Zasloff, M. (2002). Antimicrobial peptides of multicellular organisms. *Nature, 415*(6870), 389–395.